International Journal of Nanoelectronics and Materials
IJNeaM
ISSN 1985-5761 | E-ISSN 2232-1535

Fabrication and characterization of metal-organic frameworks-5 based on zinc nitrate hydrate for sodium ion battery electrodes

Sutikno Madnasri [a] *, Markus Diantoro [b], Meilody Indreswari [a], Fianti [a], Budi Astuti [a], and Ismah Lutfiyah [b]

[a]*Physics Department, Faculty of Mathematics and Natural Sciences, Universitas Negeri Semarang, Semarang, Indonesia*
[b]*Physics Department, Faculty of Mathematics and Natural Sciences, Universitas Negeri Malang, Malang, Indonesia*
** Corresponding author. Tel.: +62-24-86008700; fax: +62-24-86008700; e-mail: sutiknomadnasri@mail.unnes.ac.id*

Received 14 February 2024, Revised 15 July 2025, Accepted 12 August 2025

ABSTRACT

The growing need for renewable energy has led to an increasing demand for batteries, along with their associated technological requirements. Electrochemical storage technology depends on electrode and separator materials. The material selected for the battery electrodes is Metal Organic Frameworks (MOFs). MOFs are new materials consisting of a series of organic compounds and metal ions that form a regular pore crystal structure that can be widely applied, one of which is as a sodium ion electrode. MOFs possess unique properties that make them suitable as electrode materials for batteries, including high porosity, tunable multicomponent pore structures, and high surface areas. The aim of this study is to optimize the synthesis parameters of MOF5. MOF5 was synthesized using solvothermal methods at temperatures between 650-850 °C. Zinc nitrate tetrahydrate and acetic acid were dissolved in DMF (N, N-dimethyl formamide). The remaining precipitate (MOF) was soaked three times in DMF and three times in chloroform for 24 hours for each soaking. MOF5 samples have limited thermal resistance and degrade at high temperatures. The optimum stability of MOF5 is found at 650°C. Changes in the structure and surface morphology of MOF5 at high temperatures can impact the material's performance in battery electrode applications. The properties of MOF5 are relatively stable when used in sodium batteries, thanks to the use of a polyvinylidene fluoride (PVDF) binder and epoxy resin. For optimum binder performance, CV testing was carried out by varying the scan rate of 100 mV/s; 80 mV/s; 50 mV/s; 20 mV/s.

Keywords: *Capacitance, Cell coin, Electrode, Metal-organic framework, Sodium battery*

1. INTRODUCTION

Batteries have gained increasing attention as energy storage solutions for various applications that require portability and mobility. In the global market, the use of lithium-ion batteries remains the most dominant due to their excellent electronic energy storage capabilities [1], [2]. However, due to the limited availability of the element lithium in nature, it is now becoming increasingly scarce, causing the price of raw materials to skyrocket. Researchers are exploring alternatives to lithium, such as sodium, which is the second-lightest alkali metal and offers a more environmentally friendly option for energy storage [3]. With the increasing need for large-scale electronic energy storage systems, numerous innovations have been developed to focus on creating electrode materials for efficient battery manufacture [4]. Lithium-ion batteries are one of the electronic energy storage devices that have high gravimetric and volumetric energy densities [5], [6]. According to [7], in contrast to lithium, sodium is not limited to the earth's crust and sea, and is one of the most abundant elements in the earth's crust. The use of sodium-ion batteries, which are currently being developed, can serve as an alternative to lithium-ion batteries [8], [9]. To improve the performance of sodium-ion batteries, this can be achieved by enhancing capacity, stability, and conductivity through technological advancements in nanostructured electrodes [10].

One way to improve the performance of sodium-ion batteries is by increasing technological development in the electrode section [11], [12]. The power source of sodium battery electrodes is considered superior, with a higher capacity. Battery stability can be improved by optimizing the electrodes and electrolyte to make them more resistant to corrosion and oxidation [13], as well as increasing capacity retention over cycle life [9]. Electrode materials of interest for improving the performance of sodium ion batteries include: hard carbon for example expanded graphite [14] and carbon nanosheets [15], graphene-based materials, porous carbon nanofibers, 3D porous amorphous carbon [16] e.g. Metal-Organic Frameworks [17], biomass-derived carbon microspheres [18], [19]; intercalation-based compounds e.g. $Na_2Ti_3O_7$ [20]; $NaTi_2(PO_4)_3$ [21]; Na_xVO_2 [22]; and organic molecules and polymers [21], for example quinone and pteridine derivatives [24], n-doped polyimides [25], and sodium terephthalate [26], [27]. In addition to the hard carbon materials mentioned, Metal-Organic Frameworks (MOFs) are starting to be developed as electrodes in sodium-ion materials [9], [28].

Based on several studies, the composition and temperature can affect the energy and lifespan of sodium-ion batteries. Sodium battery electrodes are considered to have good prospects because the electrode part of a sodium-ion battery has great potential to store electrochemical energy due to its large surface area and good pore structure,

namely Metal-Organic Framework-Derived Carbons (MOFDCs) [29]. Metal-Organic Frameworks (MOFs) are three-dimensional crystalline, microporous, and hybrid nanomaterials, known as porous coordination polymers (PCP), that consist of inorganic metal groups and organic ligands [30]. Metal-organic frameworks (MOFs) exhibit high porosity with a very large surface area [31]. Porosity or void space in MOFs can be formed in various forms. Empty space is connected by channels that span higher dimensions, allowing them to penetrate solids [32]. According to [33], the free space within the pores can be accessed by inserting a pore window with a smaller diameter than the actual pore. This makes MOFs a new class of materials with a wide range of applications [34], including gas storage [35], catalysis [36], magnetism [37], and solar cells [9], among others.

MOF5 or Metal-Organic Framework 5 is a nanostructured material consisting of metal and organic ligands that can be used in various applications, including energy storage and conversion. One potential application of MOF5 is as an electrode material in sodium batteries. Research conducted by [38] has examined the chemical composition and distribution of elements on the surface of MOF5 electrodes for sodium battery applications. The reason MOF5 has potential for use as electrodes is due to its high ion storage capacity, good electrical and ionic conductivity, good chemical stability, and ease of modification.

However, MOF5 is still in the research and development stage as a sodium-ion battery electrode material. Further research is still needed to evaluate the potential of MOF5 and optimize its performance as a sodium ion battery electrode on a large scale. This research aims to develop MOF5 as a sodium-ion battery electrode material.

2. MATERIALS AND METHODS

2.1. Tools and Materials

To obtain a MOF5 sample based on zinc nitrate hydrate ($Zn(NO_3)_2.6H_2O$), a mixture of DMF (N,N-Dimethylformamide) with a molality of 73.09 g/mol 2-methylimidazole was used; acetic acid dissolved in a 100 ml measuring cup. The MOF5 mixture was poured into a 100 ml crucible, which was then baked using a furnace. After obtaining the MOF5 sample results, Scanning Electron Microscope - Electron Dispersive X-ray (SEM-EDX) Phenom ProNEX QC+. All samples were tested alternately to obtain experimental data for MOF5 samples with optimum temperature variations. Then test the binder and battery performance using Cyclic Voltammetry (CV) and Electrochemical Impedance Spectroscopy (EIS) tests.

2.2. MOF5 Synthesis

To prepare the MOF material, 1 g of zinc nitrate hydrate ($Zn(NO_3)_2.6H_2O$) and 0.1 g of acetic acid are dissolved in 40 ml of DMF (N,N-Dimethylformamide). The mixture was baked at various temperatures of 650°C, 700°C, 750°C, 800°C , and 850°C for 4 hours to precipitate the MOF particles. The particles were filtered and soaked three times in DMF (N,N-Dimethylformamide) and three times in chloroform for 24 hours each time. The particles were filtered one last time and then baked uncovered at 150°C for 2 hours, until the remaining solvent had completely evaporated.

2.3. MOF5 Battery Electrode Preparation

MOF battery electrode preparation involves preparing an MOF5 electrode slurry. Making the MOF5 electrode slurry involves using two different types of binders. The binder used is a combination of polyvinylidene fluoride (PVDF) and epoxy resin. In the PVDF binder, the MOF5 sample was synthesized using a mixture of PVDF and carbon black with dimethyl acetamide (DMAC) as the diluent. Meanwhile, in the epoxy resin binder, the MOF5 sample was synthesized with a mixture of epoxy resin, carbon black, and isopropyl alcohol (IPA) as a solvent. Stirring adjusts the thickness by adding carbon black in a regular manner.

2.4. Materials Characterization

MOF5 samples were analysed via a Phenom Pro X Scanning Electron Microscope – Electron Dispersive X-ray (SEM-EDX) imaging scan at magnifications up to 3 µm to analyse the microstructure and composition of MOF5. To determine the bonds in particles, PerkinElmer's Fourier-Transform Infrared (FTIR) spectrometer is used. Meanwhile, to determine the amount of energy using UV-VIS. Then, coin cell preparation was carried out with 2 different types of binders. Electrochemical performance testing was carried out using CV and EIS to compare optimal binder performance data. After that, CV testing was carried out with variations in scan rate on the electrode with the most optimal binder performance.

3. RESULTS AND DISCUSSION

Figure 1 indicates the structural instability of MOF5 when the temperature increases due to changes in the width pattern of each peak. The C-O peak bond undergoes symmetrical and asymmetric stretching, which indicates a bond with Zn [39]. The C-O peak appears in the wavelength range of 476cm^{-1}, which may indicate changes in the state of chemical bonds or molecular interactions in MOF5.

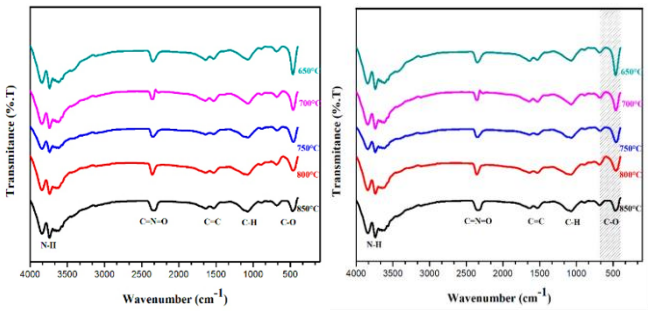

Figure 1. FTIR spectrum of the MOF5 sample resulting from heating at temperatures: a) 650°C, b) 700°C, c) 750°C, d) 800°C, and e) 850°C.

There is a small peak at a wavelength of 1071 $cm^{-1,}$ which corresponds to the C-H bond peak, indicating the presence of a benzene group with a BDC structure. The absorption formed by stretching in the MOF5 sample at 650 °C was sharper than the other high-temperature variations. The sharp absorption in this graph shows that the bond formed in the C-O group is getting stronger.

To help identify atomic bonds and functional groups in the compounds being characterized, references such as those shown in Table 1 can be used. There is a C≡N (OH stretch) bond at a wave number around 3800-3700, indicating the presence of an acetonitrile molecule [40] which has the distinctive property of a high dielectric constant because it contains an additional band placed on the low frequency side of the phenol O-H stretch band, as the nitrile concentration increases ΔvOH [41]. The wavenumber range of 1600-1500 cm-1 is the peak series for ZnO bond groups. At a wavenumber of around 1000, there are traces of C-O bonds (stretch), indicating the presence of carboxylic acid groups [42]. At a wavenumber of approximately 460, a cluster is observed [43]. Based on the results of the FTIR analysis, it is evident that MOF5 crystals have formed, as indicated by the typical absorption observed in all five samples. The shift in absorption in each graph in the sample is due to the influence of the use of DMF (N,N-Dimethylformamide), resulting in deprotonation of benzene tricarboxylic acid, which can remove the benzene ligand in the MOF5 crystal structure [44].

Table 1. Atomic Bonding and Wave Number of MOF5 Samples with High Temperature Variations

Functional group	Wavenumber	References
N - H	3740 cm^{-1}	4000 – 2800 cm^{-1} [45]
C = N = O	2357 cm^{-1}	2275 – 2250 cm^{-1}
C = C	1531 cm^{-1}	1675 – 1500 cm^{-1}
C - H	1071 cm^{-1}	1470 cm^{-1} [46]
C - O	467 cm^{-1}	1150 – 950 cm^{-1} [47]

In the UV-Vis test, as shown in Figure 2, the MOF5 sample experienced an electronic transition in the MOF5 structure. In the MOF5 sample, a peak or band is visible, which indicates the absorbance of light in a certain wavelength range. MOF5 samples subjected to temperature variations have an emission spectrum peak in the wavelength range of 360-480 nm. The higher the MOF5 temperature variation, the more unstable the emission spectrum peak shifts. This is indicated by the lower absorbance value if the temperature variation of the MOF5 sample is higher.

Where the value of the absorbance intensity formed shifts towards the blue shift in accordance with increasing temperature variations in the MOF5 sample [48], so the higher the temperature variation, the greater the wavelength at the absorption peak. To determine the optimum temperature for using the MOF5 sample in battery electrodes, it is necessary to study the MOF5 microstructure using SEM images. Based on the SEM image results, it can be observed that the crystals are not perfect. MOF5 forms crystals with an octahedral morphology so that the circle clusters on the MOF5 surface form a mesoporous structure [22]. The structure on the MOF5 surface is influenced by the boiling point of zinc, which occurs at a temperature of 800°C, so that evaporation of nano-Zn is possible at 908°C [49].

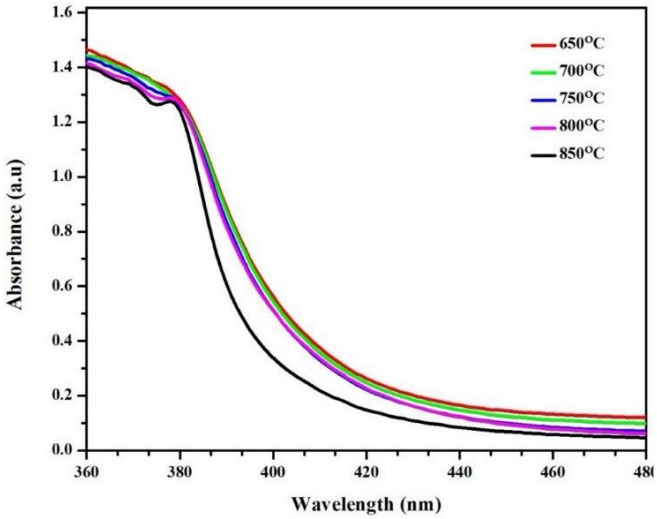

Figure 2. UV-Vis of MOF5 samples resulting from heating at temperatures: a) 650°C, b) 700°C, c) 750°C, d) 800°C, and e) 850°C.

In ZnO, the wide band gap energy is located in the UV region, with a wavelength of more than 360 cm^{-1}. The electronic transition that occurs is a ligand-to-metal charge transfer transition, which is illustrated below

$$O^2 - Zn^{2+} \rightarrow O - Zn^{+}$$

This indicates intense absorption of complex terephthalic acid, starting at 380 cm-1, with the absorption extending into the UV region. Test results indicate that MOF5 exhibits significant UV absorption at wavelengths below 300 nm. Additionally, MOF5 exhibits a broader absorption peak in the wavelength range of 300-450 nm at both room temperature and high temperatures. In MOF-5, there are two main characteristics: maximum, located at a wavelength of ≤ 380 $cm^{-1,}$ which indicates absorption of the organic portion, and ≥400$cm^{-1,}$ which indicates absorption of the inorganic portion. Test results indicate that MOF5 exhibits significant UV absorption at wavelengths below 300 nm. Additionally, MOF5 exhibits a broader absorption peak in the wavelength range of 300-450 nm at elevated temperatures. The results of the UV-Vis test indicate that MOF5 exhibits a strong ability to absorb UV light, making it suitable for use as a UV-sensitive electrode in sodium batteries. Absorption of UV light on the battery electrodes can improve battery performance by increasing the electrical conductivity and reducing the oxidation reaction of the electrodes during recharging.

MOF5 fabrication was carried out at a temperature variation of 850°C, as shown in Figures 3c) and 3d), where

maximum evaporation of zinc and carbon elements occurs so that MOF5 sample images form a collection of fibrous circles into a single structure. This indicates that near the evaporation temperature of zinc and carbon elements in the MOF5 sample at 800°C, the resulting crystal size becomes larger, and there are many collections of irregularly shaped crystal circles. SEM test results indicate that MOF5 decomposes into a porous material with a loose structure. The morphology of this material can be altered by the degree of drying, crystal properties, and decomposition temperature. The test results showed that MOF5 was degraded at temperatures above 750°C, and its crystal structure was damaged. The morphology of this material can be altered by the degree of drying, crystal properties, and decomposition temperature.

Based on the results of this SEM test, it can be concluded that MOF5 exhibits limited thermal resistance and undergoes degradation at high temperatures. Changes in the structure and surface morphology of MOF5 at temperatures above 750°C can affect the material's performance in battery electrode applications.

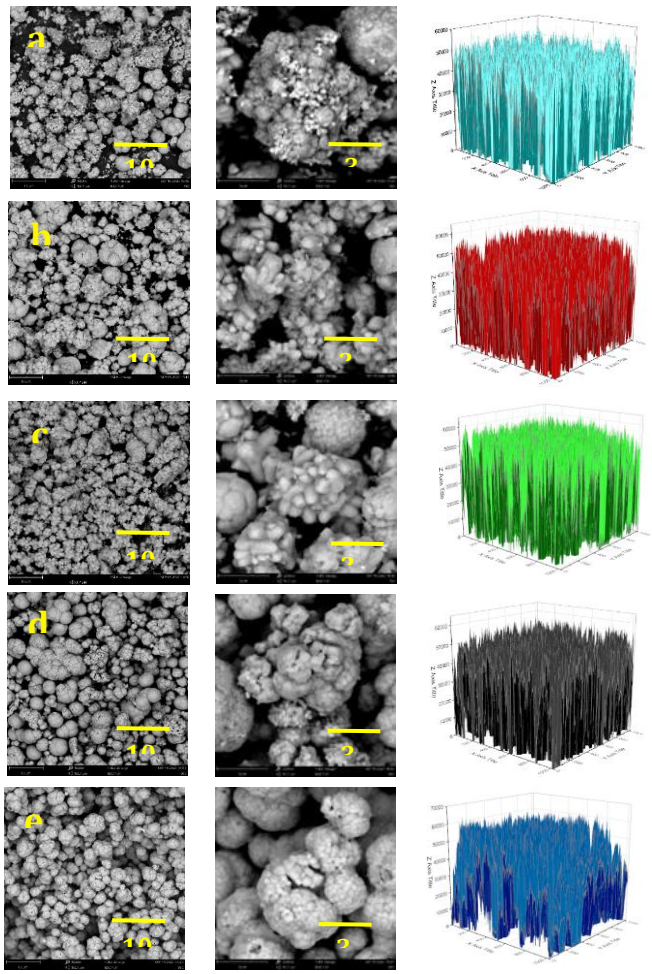

Figure 3. SEM data of MOF5 samples resulting from heating at temperatures: a) 650°C, b) 700°C, c) 750°C, d) 800°C, and e) 850°C.

Stable porosity in batteries can increase ion and electron conductivity, reduce drag and resistance, and increase battery efficiency and durability. The optimal porosity in the sample, as determined at a high temperature of 650°C, was 65%. The higher the temperature, the less optimal the porosity in the electrode and separator due to the increasing pore size. Pores that are too large can compromise the structural stability of the battery and increase electrode damage, while pores that are too small can block the flow of ions and electrolytes, thereby reducing battery capacity.

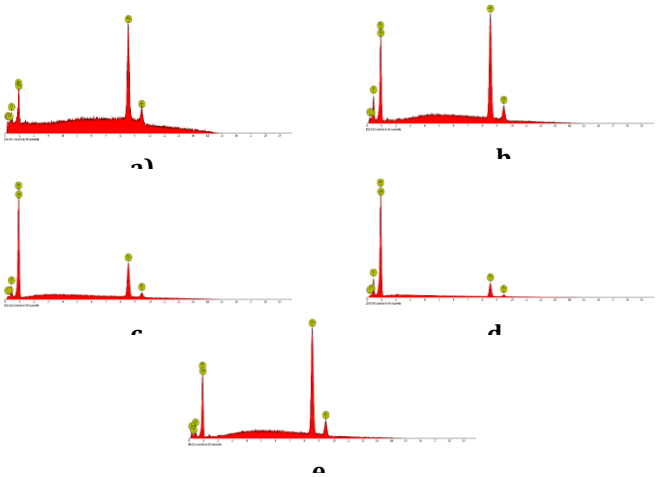

Figure 4. SEM data of MOF5 samples resulting from heating at temperatures: a) 650°C, b) 700°C, c) 750°C, d) 800°C, and e) 850°C.

Next, to identify the elements and oxides in the zinc nitrate-based MOF5 sample analyzed using EDX, Figure 4 is shown. EDX analysis was used to determine the composition and oxidation state of the MOF5 sample. Figure 4 shows that the elements read in MOF5 consist of metal (Zn), carbon (C), oxygen (O), and copper (Cu), which corresponds to the composition of the MOF5 material. The EDX test results showed that the distribution of elements on the surface of the MOF5 electrode was uniform, with the weight composition of the Zn element at different temperatures, namely at a temperature of 650°C of 75%wt, a temperature of 700°C of 65%wt, a temperature of 750°C of 60%wt, a temperature of 800°C of 60%wt, and a temperature of 850°C of 60%wt.

Table 2. EDX analysis results of MOF5 crystals.

		Weight Composition (%wt)				
No	Element	MOF5 650°C	MOF5 700°C	MOF5 750°C	MOF5 800°C	MOF5 850°C
1	Zn	93.98	92.78	82.17	81.87	80.44
2	C	2.62	2.28	2.92	1.49	4.52
3	O	2.09	3.86	11.16	12.41	1.49
4	N	1.30	1.07	3.75	4.22	0.99

Table 2 shows the elemental composition of metal (Zn), carbon (C), oxygen (O), and copper (Cu) at several MOF5

crystal points from the five samples. The results were relatively uniform and constant for each elemental composition of the crystal. The most dominant element is metal (Zn). This ensures that the quality and homogeneity of the MOF5 electrode are quite stable in sodium battery applications. If the distribution of elements in the sample is not uniform, it can disrupt the electrode's performance and lead to a decrease in battery life.

The battery binder is a component of the coin cell battery, serving as an adhesive for the active material on the battery electrodes. The choice of binder type will impact the ability to bind the active material to the electrode, resulting in a dense and stable structure. CV testing is conducted within a potential window of 0–500 mV and at a pulse rate of 1 mV/s, yielding data on the relationship between voltage (V) and current (I). The results of electrochemical property measurements using CV on the use of 2 different types of binders, namely PVDF and epoxy, are shown in Figure 5.

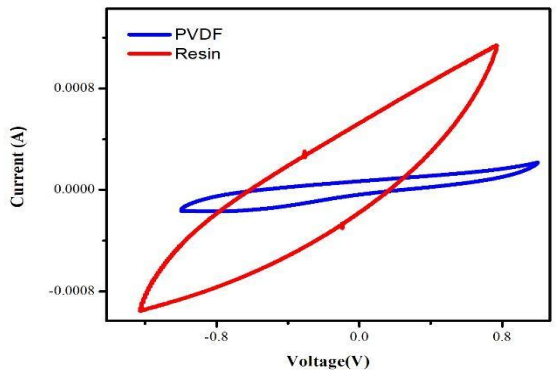

Figure 5. CV Spectrum of MOF5 Sample Cell Coin with PVDF Binder and Epoxy Resin.

The area of the electrode using the epoxy resin binder is larger than that of the electrode using the PVDF binder. Table 3 mathematically demonstrates that the coin cell area with a PVDF binder is 0.202 mm smaller than the coin cell area with an epoxy resin binder, which is 0.616 mm. This is reinforced by the specific capacitance value, which indicates the energy storage capacity that can be contained in each gram of the sample [50]. The specific capacitance in the coin cell area with a PVDF binder is 0.19 Fg^{-1}, which is smaller than the specific capacitance in the coin cell area with an epoxy resin binder of 0.59 Fg^{-1}. This happens because the higher the capacitance, the more electrical charge the battery can store, and the longer the battery can last before needing to be recharged.

Table 3. CV Analysis of MOF5 Sample Cell Coins with PVDF Binder and Epoxy Resin.

No	Binder	Area (Q)	Specific Capacitance (Fg^{-1})	Energy Density (Whg^{-1})
1	PVDF	0,202	0,19	10,52
2	Resin	0,616	0,59	3,38

This is proven by mathematical calculations of the relation between the area and the specific capacitance of the coin cell with the equation:

$$C = \frac{1}{2 \times v \times \Delta m \times \Delta V} \int I \, dv$$

$$ED = \frac{1}{2} C_S (\Delta V)^2 = \frac{1}{2} \frac{C}{m} (\Delta V)^2$$

The energy density in the coin cell area with PVDF binder is 10.52 Whg^{-1}, which is smaller than that of the coin cell area with epoxy resin binder, which is 3.38 Whg^{-1}. Energy density refers to the amount of energy a battery can store per unit of mass, while power density describes how quickly a battery can provide electrical power.

Epoxy resin binders are considered more optimal because they can help increase energy density by optimizing overall battery capacity. By ensuring that the active material particles on the electrodes remain firmly and stably bound, batteries can store more energy by optimizing the surface area that participates in chemical reactions during charging and discharging.

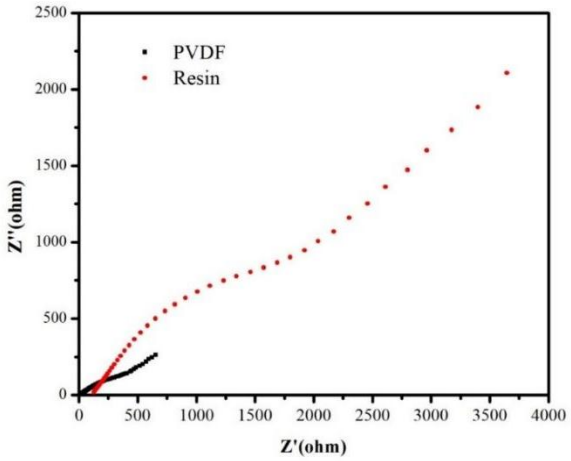

Figure 6. EIS spectrum of the MOF5 sample coin cell with PVDF binder and epoxy resin.

The EIS graph in Figure 6 shows that the electrode area with a resin binder is larger than that with a PVDF binder. The information about capacitance in the EIS test results on coin cell batteries has some important relevance. First, capacitance is a crucial indicator of battery performance, particularly in terms of battery capacity and electrode response. An increase or decrease in capacitance may indicate a change in battery performance or a problem that requires attention. Second, capacitance can help in understanding the electrochemical processes that occur in batteries, such as diffusion processes, charge transfer, and electrode reactions. So, the EIS data shows that the electrochemical performance of the coin cell is better using epoxy.

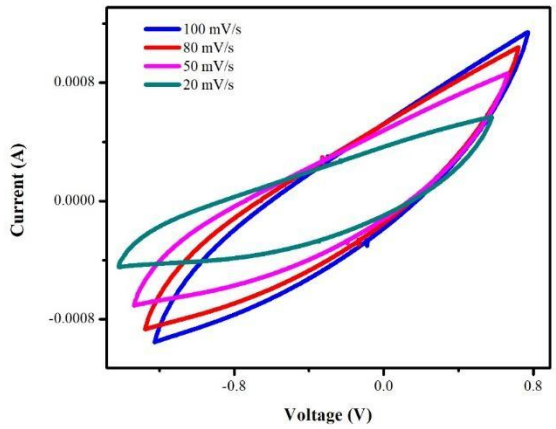

Figure 7. CV Spectrum of Coin Cells for MOF5 Epoxy Resin Binder Samples with Varying Scan Rates.

The scan rate variations were conducted using an epoxy resin binder. The results of the CV spectrum of the MOF5 sample coin cell are obtained as shown in Figure 7. The CV spectrum indicates that a scan rate of 100 mV/s is considered more optimal, as it can help increase the specific capacitance and energy density.

Table 3 shows mathematically that the area of a coin cell with a scan rate of 100 mV/s is 0.109 larger than a coin cell with a scan rate of 80 mV/s; 5 0 mV/s; 20 mV/s of 0.105; 0.095; 0.073. This is reinforced by the specific capacitance value, which indicates the energy storage capacity that can be contained in each gram of the sample [50]. Where the specific capacitance in the coin cell area of a coin cell with a scan rate of 100 mV/s is 0.308 $Fg^{-1,}$ greater than a coin cell with a scan rate of 80 mV/s; 5 0 mV/s; 20 mV/s of 0.370 Fg^{-1}; 0.535 Fg^{-1}; 0.103 Fg^{-1}. This happens because the higher the capacitance, the more electrical charge the battery can store, and the longer the battery can last before needing to be recharged.

CONCLUSION

The manufacture of sodium-ion batteries by exploring zinc nitrate-based hard carbon metal-organic frameworks (MOFs) can yield quite high solid crystallinity results at each temperature variation. The varied temperature determines the character of the microstructure, which exhibits high porosity with a very large surface area at temperatures of 650°C and 700°C. This is evident in the MOF5 crystals, which are almost perfectly octahedral. The higher the temperature, the smaller the crystal structure, and the more irregular it becomes. This is influenced by the boiling point of zinc, which occurs at a temperature of 800°C, so that the evaporation of the heavy composition of the zinc element is reduced. The composition of MOF5 shows a series of peaks for the ZnO bond group, which experiences an absorption shift due to the influence of the use of DMF (N,N-Dimethylformamide). So that the crystal structure in the form of benzene ligands will be deprotonated. The shift in the peak series also shows intense absorption in the terephthalic acid complex, which results in electronic transitions with charge transfer from the ligand to the metal.

ACKNOWLEDGMENTS

We would like to thank the Ministry of Education, Culture, Research and Technology of the Republic of Indonesia for funding this research through the 2023 National Competitive Fundamental Research Grant Scheme under contract 3.15.6/UN37/PPK.10/2023.

REFERENCES

[1] J. Wu, M. A. Hughes, N. Sharma, and J. Allen, "Influence of Growth Parameters on the Electrochemical Performance of Electrodeposited Carbons," *Batteries*, vol. 8, no. 8, Aug. 2022, doi: 10.3390/batteries8080081.

[2] J.-M. Tarascon and M. Armand, "Issues and challenges facing rechargeable lithium batteries," 2001. [Online]. Available: www.nature.com

[3] F. Markoulidis, A. Dawe, and C. Lekakou, "Electrochemical double-layer capacitors with lithium-ion electrolyte and electrode coatings with PEDOT:PSS binder," *J Appl Electrochem*, vol. 51, no. 3, pp. 373–385, Mar. 2021, doi: 10.1007/s10800-020-01497-y.

[4] J. M. Lee, C. Choi, J. H. Kim, M. J. de Andrade, R. H. Baughman, and S. J. Kim, "Biscrolled Carbon Nanotube Yarn Structured Silver-Zinc Battery," *Sci Rep*, vol. 8, no. 1, Dec. 2018, doi: 10.1038/s41598-018-29266-0.

[5] M. Baumann, J. F. Peters, M. Weil, and A. Grunwald, "CO2 Footprint and Life-Cycle Costs of Electrochemical Energy Storage for Stationary Grid Applications," *Energy Technology*, vol. 5, no. 7, pp. 1071–1083, Jul. 2017, doi: 10.1002/ente.201600622.

[6] T. Ma *et al.*, "A review of organic sulfur applications in lithium-sulfur batteries," Jan. 01, 2025, *Elsevier B.V.* doi: 10.1016/j.jpowsour.2024.235717.

[7] K. Karuppasamy *et al.*, "Nanostructured transition metal sulfide/selenide anodes for high-performance sodium-ion batteries," in *Nanostructured, Functional, and Flexible Materials for Energy Conversion and Storage Systems*, Elsevier, 2020, pp. 437–464. doi: 10.1016/B978-0-12-819552-9.00014-2.

[8] D. Kundu, E. Talaie, V. Duffort, and L. F. Nazar, "The emerging chemistry of sodium ion batteries for electrochemical energy storage," Mar. 09, 2015, *Wiley-VCH Verlag*. doi: 10.1002/anie.201410376.

[9] Y. Li, A. Pang, C. Wang, and M. Wei, "Metal-organic frameworks: Promising materials for improving the open circuit voltage of dye-sensitized solar cells," *J Mater Chem*, vol. 21, no. 43, pp. 17259–17264, Nov. 2011, doi: 10.1039/c1jm12754c.

[10] J. F. Peters, A. P. Cruz, and M. Weil, "Exploring the economic potential of sodium-ion batteries," *Batteries*, vol. 5, no. 1, Mar. 2019, doi: 10.3390/batteries5010010.

[11] J. Deng, W. Bin Luo, S. L. Chou, H. K. Liu, and S. X. Dou, "Sodium-Ion Batteries: From Academic Research to Practical Commercialization," Feb. 05, 2018, *Wiley-VCH Verlag*. doi: 10.1002/aenm.201701428.

[12] S. Madnasri and L. Ati, "Organic Solar Cell Performance of Musa acuminata bracts Extract by Microwave Irradiation Treatment," *Int J Energy Res*, vol. 45, no. 3, pp. 4214–4223, 2021.

[13] X. Zheng, C. Bommier, W. Luo, L. Jiang, Y. Hao, and Y. Huang, "Sodium metal anodes for room-temperature sodium-ion batteries: Applications, challenges and solutions," Jan. 01, 2019, *Elsevier B.V.* doi: 10.1016/j.ensm.2018.04.014.

[14] J. Ding *et al.*, "Carbon nanosheet frameworks derived from peat moss as high performance sodium ion battery anodes," *ACS Nano*, vol. 7, no. 12, pp. 11004–11015, Dec. 2013, doi: 10.1021/nn404640c.

[15] H. G. Wang *et al.*, "Nitrogen-doped porous carbon nanosheets as low-cost, high-performance anode material for sodium-ion batteries," *ChemSusChem*, vol. 6, no. 1, pp. 56–60, Jan. 2013, doi: 10.1002/cssc.201200680.

[16] P. Lu, Y. Sun, H. Xiang, X. Liang, and Y. Yu, "3D Amorphous Carbon with Controlled Porous and Disordered Structures as a High-Rate Anode Material for Sodium-Ion Batteries," *Adv Energy Mater*, vol. 8, no. 8, Mar. 2018, doi: 10.1002/aenm.201702434.

[17] D. Liu *et al.*, "3D printing of metal-organic frameworks decorated hierarchical porous ceramics for high-efficiency catalytic degradation," *Chemical Engineering Journal*, vol. 397, Oct. 2020, doi: 10.1016/j.cej.2020.125392.

[18] Y. Li *et al.*, "Amorphous monodispersed hard carbon micro-spherules derived from biomass as a high performance negative electrode material for sodium-ion batteries," *J Mater Chem A Mater*, vol. 3, no. 1, pp. 71–77, Jan. 2015, doi: 10.1039/c4ta05451b.

[19] Sutikno, I. Yulianti, and D. Saputera, "An investigation of pH effects on the properties of the fabricated banana flower extracts-based organic solar cell," *Oriental Journal of Chemistry*, vol. 33, no. 1, pp. 318–323, 2017.

[20] A. Rudola, K. Saravanan, C. W. Mason, and P. Balaya, "Na2Ti3O7: An intercalation based anode for sodium-ion battery applications," *J Mater Chem A Mater*, vol. 1, no. 7, pp. 2653–2662, Feb. 2013, doi: 10.1039/c2ta01057g.

[21] X. Wu, Y. Cao, X. Ai, J. Qian, and H. Yang, "A low-cost and environmentally benign aqueous rechargeable sodium-ion battery based on NaTi2(PO4)3-Na 2NiFe(CN)6 intercalation chemistry," *Electrochem commun*, vol. 31, pp. 145–148, Jun. 2013, doi: 10.1016/j.elecom.2013.03.013.

[22] C. Deng, S. Zhang, Z. Dong, and Y. Shang, "1D nanostructured sodium vanadium oxide as a novel anode material for aqueous sodium ion batteries," *Nano Energy*, vol. 4, pp. 49–55, Mar. 2014, doi: 10.1016/j.nanoen.2013.12.014.

[23] Q. Zhao, Y. Lu, and J. Chen, "Advanced Organic Electrode Materials for Rechargeable Sodium-Ion Batteries," Apr. 19, 2017, *Wiley-VCH Verlag*. doi: 10.1002/aenm.201601792.

[24] Y. Liang *et al.*, "Universal quinone electrodes for long cycle life aqueous rechargeable batteries," *Nat Mater*, vol. 16, no. 8, pp. 841–848, Aug. 2017, doi: 10.1038/nmat4919.

[25] H. Qin, Z. P. Song, H. Zhan, and Y. H. Zhou, "Aqueous rechargeable alkali-ion batteries with polyimide anode," *J Power Sources*, vol. 249, pp. 367–372, 2014, doi: 10.1016/j.jpowsour.2013.10.091.

[26] Y. Park *et al.*, "Sodium terephthalate as an organic anode material for sodium ion batteries," *Advanced Materials*, vol. 24, no. 26, pp. 3562–3567, Jul. 2012, doi: 10.1002/adma.201201205.

[27] T. Adam, U. Hashim, and S. Madnasri, "Simulation of passive fluid driven micromixer for fast reaction assays in nano lab-on-chip domain," *Procedia Eng*, vol. 50, pp. 416–425, 2012.

[28] W. Xia, A. Mahmood, R. Zou, and Q. Xu, "Metal-organic frameworks and their derived nanostructures for electrochemical energy storage and conversion," Jul. 01, 2015, *Royal Society of Chemistry*. doi: 10.1039/c5ee00762c.

[29] N. Ingersoll, Z. Karimi, D. Patel, R. Underwood, and R. Warren, "Metal organic framework-derived carbon structures for sodium-ion battery anodes," *Electrochim Acta*, vol. 297, pp. 129–136, Feb. 2019, doi: 10.1016/j.electacta.2018.11.140.

[30] J. A. Bohrman and M. A. Carreon, "Synthesis and CO2/CH4 separation performance of Bio-MOF-1 membranes," *Chemical Communications*, vol. 48, no. 42, pp. 5130–5132, Apr. 2012, doi: 10.1039/c2cc31821k.

[31] N. Klein *et al.*, "A mesoporous metal-organic framework," *Angewandte Chemie - International Edition*, vol. 48, no. 52, pp. 9954–9957, Dec. 2009, doi: 10.1002/anie.200904599.

[32] O. I. Lebedev, F. Millange, C. Serre, G. Van Tendeloo, and G. Férey, "First direct imaging of giant pores of the metal-organic framework MIL-101," *Chemistry of Materials*, vol. 17, no. 26, pp. 6525–6527, Dec. 2005, doi: 10.1021/cm051870o.

[33] R. Scott Morris and B. G. Dixon, "A novel approach for development of improved polymer electrolytes for lithium batteries," in *Journal of Power Sources*, Jun. 2003, pp. 487–491. doi: 10.1016/S0378-7753(03)00270-2.

[34] T. Pham, K. A. Forrest, B. Space, and J. Eckert, "Dynamics of H2 adsorbed in porous materials as revealed by computational analysis of inelastic neutron scattering spectra," 2016, *Royal Society of Chemistry*. doi: 10.1039/c6cp01863g.

[35] E. Tsivion, J. A. Mason, M. I. Gonzalez, J. R. Long, and M. Head-Gordon, "A computational study of CH4 storage in porous framework materials with metalated linkers: Connecting the atomistic character of CH4 binding sites to usable capacity,"

Chem Sci, vol. 7, no. 7, pp. 4503–4518, 2016, doi: 10.1039/c6sc00529b.

[36] P. García-García, M. Müller, and A. Corma, "MOF catalysis in relation to their homogeneous counterparts and conventional solid catalysts," *Chem Sci*, vol. 5, no. 8, pp. 2979–3007, 2014, doi: 10.1039/c4sc00265b.

[37] E. Coronado and G. M. Espallargas, "Dynamic magnetic MOFs," *Chem Soc Rev*, vol. 42, no. 4, pp. 1525–1539, Jan. 2013, doi: 10.1039/c2cs35278h.

[38] S. Madnasri *et al.*, "Synthesis and Characterization of Metal-Organic Framework as Battery Electrodes," *Jurnal Bahan Alam Terbarukan*, vol. 12, no. 1, pp. 78–86, Jun. 2023, doi: 10.15294/jbat.v12i1.44170.

[39] R. Sabouni, H. Kazemian, and S. Rohani, "A novel combined manufacturing technique for rapid production of IRMOF-1 using ultrasound and microwave energies," *Chemical Engineering Journal*, vol. 165, no. 3, pp. 966–973, Dec. 2010, doi: 10.1016/j.cej.2010.09.036.

[40] A. Wilk *et al.*, "Substrate-integrated hollow waveguides: A new level of integration in mid-infrared gas sensing," *Anal Chem*, vol. 85, no. 23, pp. 11205–11210, Dec. 2013, doi: 10.1021/ac402391m.

[41] E. S. Kryachko and M. T. Nguyen, "Hydrogen bonding between phenol and acetonitrile," *Journal of Physical Chemistry A*, vol. 106, no. 16, pp. 4267–4271, Apr. 2002, doi: 10.1021/jp020423i.

[42] B. C. Smith, "The C=O Bond, Part VI: Esters and the Rule of Three," *Spectroscopy*, vol. 33, no. 7, pp. 20–23, Jul. 2018.

[43] C. R. Young *et al.*, "Infrared hollow waveguide sensors for simultaneous gas phase detection of benzene, toluene, and xylenes in field environments," *Anal Chem*, vol. 83, no. 16, pp. 6141–6147, Aug. 2011, doi: 10.1021/ac1031034.

[44] Z. Wang, L. Qie, L. Yuan, W. Zhang, X. Hu, and Y. Huang, "Functionalized N-doped interconnected carbon nanofibers as an anode material for sodium-ion storage with excellent performance," *Carbon N Y*, vol. 55, pp. 328–334, Apr. 2013, doi: 10.1016/j.carbon.2012.12.072.

[45] O. P. Dvoryaninova, A. V. Sokolov, O. V. Peregonchaya, E. A. Solovyeva, and D. A. Syanov, "Identification of composition and structure of functional groups of ferment lysates based on IR spectroscopy," in *IOP Conference Series: Earth and Environmental Science*, IOP Publishing Ltd, Feb. 2021. doi: 10.1088/1755-1315/640/3/032062.

[46] L. Đorđević *et al.*, "Design principles of chiral carbon nanodots help convey chirality from molecular to nanoscale level," *Nat Commun*, vol. 9, no. 1, Dec. 2018, doi: 10.1038/s41467-018-05561-2.

[47] B. Xing *et al.*, "Facile synthesis of graphene nanosheets from humic acid for supercapacitors," *Fuel Processing Technology*, vol. 165, pp. 112–122, 2017, doi: 10.1016/j.fuproc.2017.05.021.

[48] S. Wu *et al.*, "Linker Engineering toward Full-Color Emission of UiO-68 Type Metal-Organic Frameworks," *J Am Chem Soc*, vol. 143, no. 28, pp. 10547–10552, Jul. 2021, doi: 10.1021/jacs.1c04810.

[49] R. Guo *et al.*, "Engineering Mesoporous Structure in Amorphous Carbon Boosts Potassium Storage with High Initial Coulombic Efficiency," *Nanomicro Lett*, vol. 12, no. 1, Jul. 2020, doi: 10.1007/s40820-020-00481-7.

[50] E. Frackowiak and F. Beguin, "Carbon materials for the electrochemical storage of energy in capacitors," 2001.